PNAS RESEARCH ARTICLE | MICROBIOLOGY

5-methylcytosine (m^5C) RNA modification controls the innate immune response to virus infection by regulating type I interferons

Yuexiu Zhang[a,1], Li-Sheng Zhang[b,c,d,1], Qing Dai[b,c,d], Phylip Chen[e], Mijia Lu[a], Elizabeth L. Kairis[a], Valarmathy Murugaiah[a], Jiayu Xu[a], Rajni Kant Shukla[a], Xueya Liang[a], Zhongyu Zou[b,c,d], Estelle Cormet-Boyaka[a], Jianming Qiu[f], Mark E. Peeples[e,g], Amit Sharma[a,h], Chuan He[b,c,d,i,2], and Jianrong Li[a,2]

Edited by Howard Chang, Stanford University, Stanford, CA; received December 26, 2021; accepted August 23, 2022

5-methylcytosine (m^5C) is one of the most prevalent modifications of RNA, playing important roles in RNA metabolism, nuclear export, and translation. However, the potential role of RNA m^5C methylation in innate immunity remains elusive. Here, we show that depletion of NSUN2, an m^5C methyltransferase, significantly inhibits the replication and gene expression of a wide range of RNA and DNA viruses. Notably, we found that this antiviral effect is largely driven by an enhanced type I interferon (IFN) response. The antiviral signaling pathway is dependent on the cytosolic RNA sensor RIG-I but not MDA5. Transcriptome-wide mapping of m^5C following NSUN2 depletion in human A549 cells revealed a marked reduction in the m^5C methylation of several abundant noncoding RNAs (ncRNAs). However, m^5C methylation of viral RNA was not noticeably altered by NSUN2 depletion. In NSUN2-depleted cells, the host RNA polymerase (Pol) III transcribed ncRNAs, in particular RPPH1 and 7SL RNAs, were substantially up-regulated, leading to an increase of unshielded 7SL RNA in cytoplasm, which served as a direct ligand for the RIG-I–mediated IFN response. In NSUN2-depleted cells, inhibition of Pol III transcription or silencing of RPPH1 and 7SL RNA dampened IFN signaling, partially rescuing viral replication and gene expression. Finally, depletion of NSUN2 in an ex vivo human lung model and a mouse model inhibits viral replication and reduces pathogenesis, which is accompanied by enhanced type I IFN responses. Collectively, our data demonstrate that RNA m^5C methylation controls antiviral innate immunity through modulating the m^5C methylome of ncRNAs and their expression.

5-methylcytosine | innate immune response | virus infection | interferon

RNA methylation is a widespread posttranslational modification of RNA that regulates numerous biological processes (1–5). Among more than 170 types of RNA methylation, 5-methylcytosine (m^5C), in which the fifth carbon of cytosine is methylated, is one of the prevalent RNA modifications. The recent development of next-generation sequencing approaches such as RNA bisulfite sequencing, m^5C RNA immunoprecipitation sequencing (m^5C-RIP-seq), 5-azacytidine–mediated RNA immunoprecipitation sequencing (Aza-IP-seq), and methylation individual-nucleotide-resolution crosslinking and immunoprecipitation sequencing (miCLIP-seq) has enabled transcriptome-wide mapping of m^5C methylation (6–13). The m^5C methylation has been found in diverse RNA species including transfer RNA (tRNA), ribosomal RNA (rRNA), messenger RNA (mRNA), vault RNA (vtRNA), small nuclear RNA (snRNA), small nucleolar RNA (snoRNA), microRNA (miRNA), and viral RNA (9–13).

The m^5C modification is catalyzed by RNA m^5C methyltransferases (writers), the superfamily of Rossman fold–containing enzymes, using *S*-adenosyl-L-methionine (SAM) as a methyl donor (14). Several m^5C-specific methyltransferases, including members of the NOL1/NOP2/SUN domain (NSUN) family of proteins, which contain seven members (NSUN1–7) in humans, as well as the DNA methyltransferase (DNMT) homolog DNMT2, have been identified and characterized (14–16). Among the NSUN family, NSUN2 is one of the most well-characterized members and is a major m^5C writer (14, 15, 17). The biological function of m^5C methylation can be mediated by m^5C-binding proteins (readers), such as ALYREF and YBX1, which bind preferentially to m^5C sites in RNA (10, 18, 19). Recent studies suggest that m^5C cytosine methylation affects a wide range of cellular processes such as nuclear RNA export, mRNA translation, cell cycle control, (stem) cell differentiation and proliferation, development, and cancers (1, 8–10, 20, 21). Despite these studies, the functional consequences of m^5C methylation of RNA in cellular process are still poorly understood.

Significance

5-methylcytosine (m^5C) is a common RNA methylation. However, its biological functions remain a mystery. Here, we discover that depletion of NSUN2, an m^5C methyltransferase, leads to an enhanced type I interferon (IFN) response, which significantly inhibits replication of a wide range of RNA and DNA viruses in vitro. Notably, this m^5C-mediated antiviral innate immunity is also conserved in an in vivo mouse model. Mechanistically, depletion of the m^5C methyltransferase decreases the host RNA m^5C methylome and enhances polymerase III–transcribed noncoding RNAs that are recognized by RIG-I to trigger enhanced type I IFN signaling. Our study reveals a role of m^5C in regulating innate immunity and highlights m^5C as a new target for development of broad-spectrum antiviral therapeutics.

Competing interest statement: C.H. is a scientific founder of Accent Therapeutics, Ins. J.L. and C.H. are filing a provision patent application, 21-T-003/IDF050556.

This article is a PNAS Direct Submission.

[1]Y.Z. and L.-S.Z. contributed equally to this work.

[2]To whom correspondence may be addressed. Email: li.926@osu.edu or chuanhe@uchicago.edu.

This article contains supporting information online at http://www.pnas.org/lookup/suppl/doi:10.1073/pnas.2123338119/-/DCSupplemental.

Published October 14, 2022.

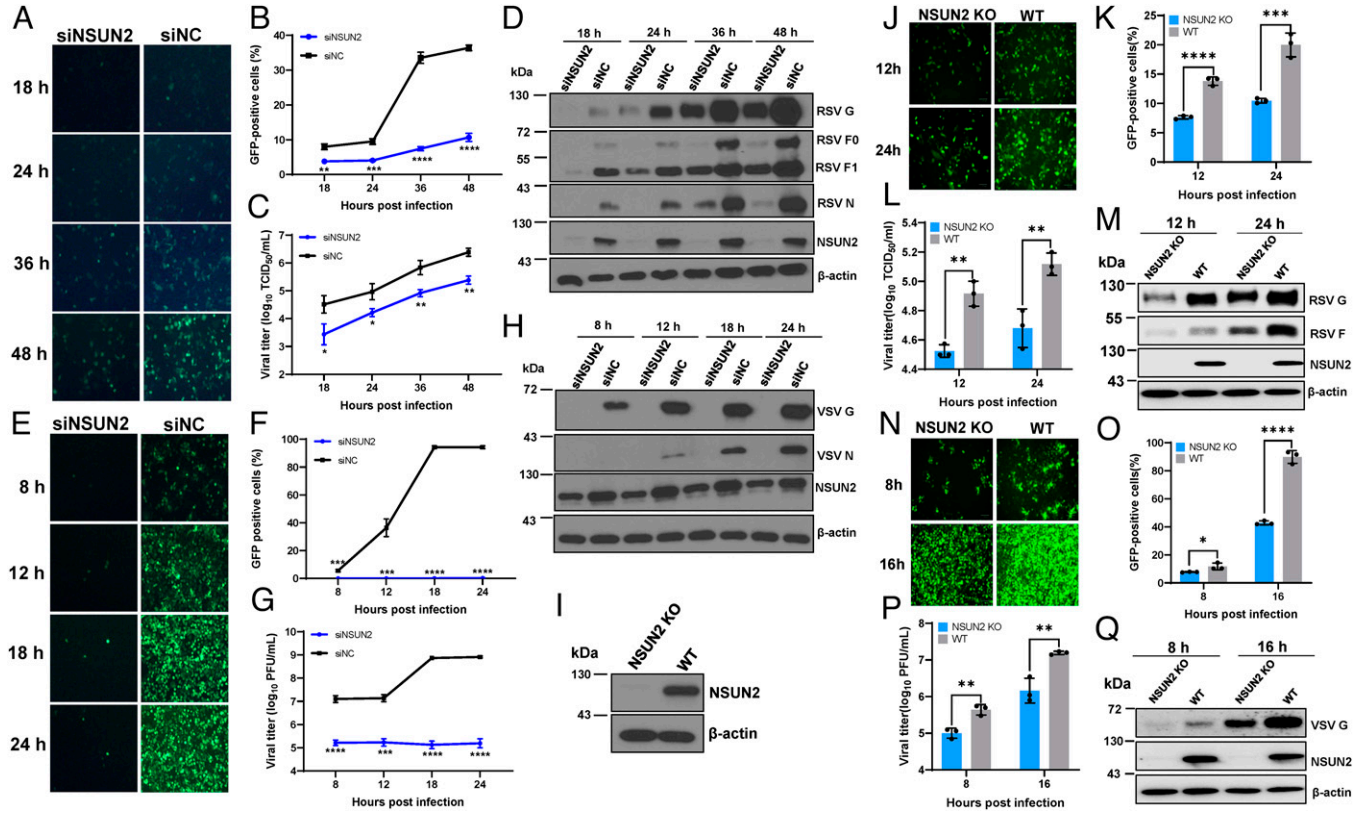

Fig. 1. NSUN2 depletion suppresses viral replication and gene expression. NSUN2 depletion suppresses RSV (*A–D*) and VSV (*E–H*) replication. A549 cells were transfected with siNSUN2 or siRNA negative control (siNC). After 24 h, cells were infected with GFP-expressing viruses (rgRSV or rVSV-GFP) at an MOI of 0.1, GFP expression was captured by fluorescence microscopy (*A* and *E*), and GFP-positive cells were quantified by flow cytometry (*B* and *F*). A single-step growth curve shows the release of RSV (*C*) and VSV (*G*). Total cell extracts were harvested from rgRSV (*D*)- or rVSV-GFP (*H*)–infected A549 cells and subjected to Western blot (*D* and *H*). (*I*) Western blot showing KO of NSUN2 in A549 cells. (*J–Q*) NSUN2 KO suppresses RSV and VSV replication. NSUN2-KO A549 cells or control sgRNA A549 cells were infected with rgRSV (*J–M*) or rVSV-GFP (*N–Q*) at an MOI of 0.1. GFP images were captured (*J* and *N*), percent of GFP-positive cells was quantified (*K* and *O*), RSV (*M*) or VSV (*Q*) protein expression was determined by Western blot, and RSV (*L*) and VSV (*P*) titers were determined. All results are from three independent experiments. Data were analyzed using Student's *t* test (*$P < 0.05$, **$P < 0.01$, ***$P < 0.001$, ****$P < 0.0001$).

Viruses are obligate intracellular parasites and rely on the host machinery to synthesize their genetic materials. The m^5C methylation in viral RNA was discovered in Sindbis virus 26S RNA in 1975 (22). Similarly, mRNA of adenovirus, a DNA virus, was shown to be m^5C modified in 1976 (23). However, biological functions of viral m^5C methylation remained a mystery for decades. Recent studies showed that NSUN2 is the primary m^5C writer of HIV-1 genome RNA (24) and m^5C in viral RNA can regulate viral mRNA translation (24, 25), RNA alternative splicing (24), RNA stability (24, 26, 27), and RNA export (28). To date, the mechanisms by which m^5C regulates viral replication and gene expression remain unclear and the role of m^5C methylation in innate antiviral immunity remains elusive.

Here we describe a role of m^5C methylation in antiviral innate immunity. Specifically, NSUN2-mediated RNA m^5C methylation controls type I interferon (IFN) responses through modulating m^5C methylome of host noncoding RNAs (ncRNAs) and their expression.

Results

Depletion of NSUN2, an m^5C Methyltransferase, Significantly Suppresses Replication and Gene Expression of a Wide Range of Viruses. To begin to explore the role of m^5C methylation in viral replication and gene expression, we first knocked down NSUN2 in A549 cells, followed by infection with several RNA viruses (human respiratory syncytial virus [RSV], vesicular stomatitis virus [VSV], human metapneumovirus [hMPV], and Sendai virus [SeV]) and a DNA virus (herpes simplex virus [HSV]). Knockdown of NSUN2 significantly reduced the replication and gene expression of all these viruses (Fig. 1 and *SI Appendix*, Fig. S1). Next, we selected VSV, RSV, and hMPV to further characterize the phenotype. Knockdown of NSUN2 led to 1.5 to 4.0 log reductions in virus titer (Fig. 1 *C* and *G* and *SI Appendix*, Fig. S1*E*) and a significant reduction in viral protein synthesis (Fig. 1 *D* and *H* and *SI Appendix*, Fig. S1*F*), viral genome replication (*SI Appendix*, Fig. S1 *G* and *H*), and mRNA transcription (*SI Appendix*, Fig. S1 *I–K*). We also generated an NSUN2-knockout (KO) A549 cell line (Fig. 1*I*) and tested viral replication. Replication and gene expression levels of RSV (Fig. 1 *J–M*) and VSV (Fig. 1 *N–Q*) were strongly inhibited in the NSUN2-KO A549 cells compared to the wild-type (WT) A549 cells. Next, NSUN2-KO A549 cells were transfected with empty vector (EV) or pCAGGS-NSUN2. As expected, RSV (Fig. 2*A*), hMPV (Fig. 2*B*), and VSV (Fig. 2 *C–E*) viral protein synthesis and viral titer were rescued by transient expression of exogenous NSUN2 protein. The functions of m^5C methylation are mediated by m^5C binding proteins (or readers) such as YBX1 and ALYREF (28). Thus, we knocked down YBX1 or ALYREF by small interfering RNA (siRNA), followed by recombinant VSV expressing green fluorescent protein (rVSV-GFP) infection. We did not observe an obvious reduction in VSV replication and gene expression in YBX1 or ALYREF-depleted A549 cells (*SI Appendix*, Fig. S2). Collectively, these results demonstrate that NSUN2 positively regulates viral replication and gene expression.

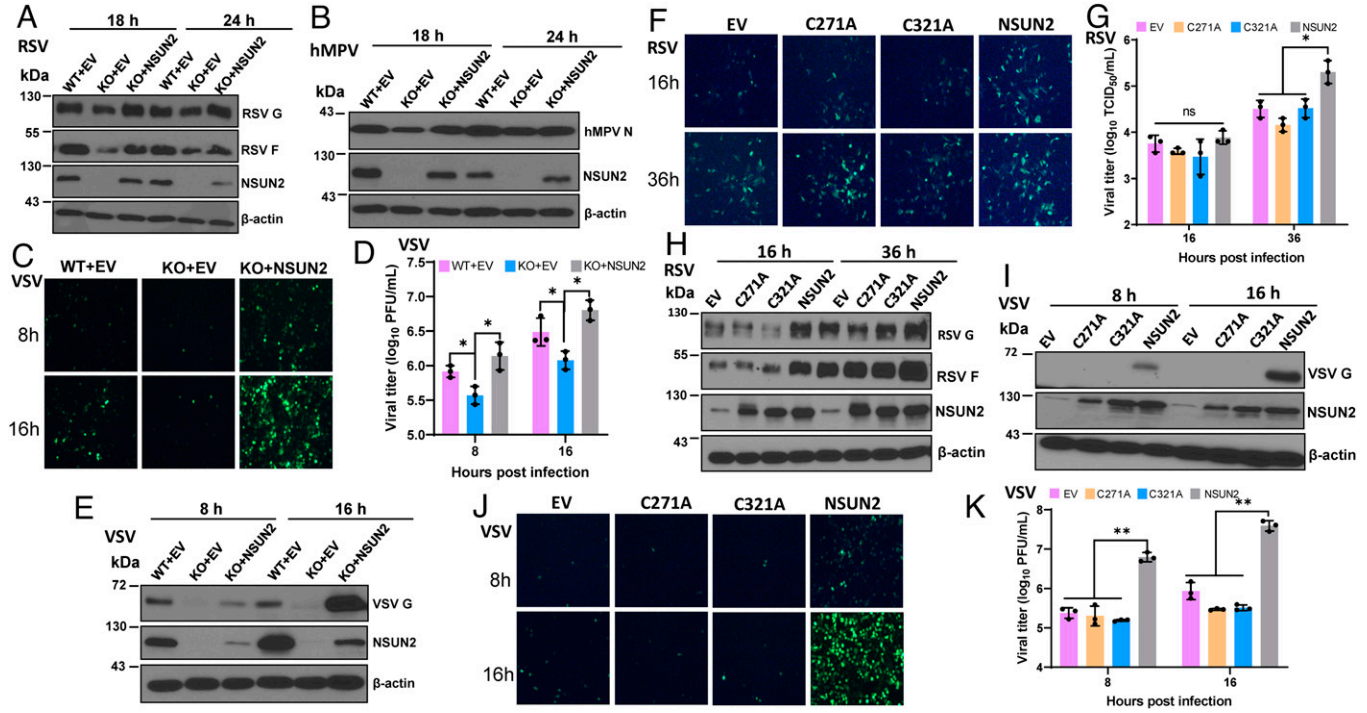

Fig. 2. m^{5}C methyltransferase of NSUN2 is essential for its proviral activity. (*A*–*E*) Rescue of viral replication and gene expression by transfection of NSUN2 plasmid. NSUN2-KO or control A549 cells were transfected with 1 μg of empty vector (EV) pCAGGS or pCAGGS-NSUN2, followed by infection with rgRSV (*A*), hMPV (*B*), or VSV (*C*–*E*) at an MOI of 1.0. Transfection of pCAGGS-NSUN2 rescued RSV (*A*), hMPV (*B*), and VSV (*E*) protein expression, as well as GFP expression by rVSV-GFP (*C*) and VSV titer (*D*). (*F*–*K*) Two cysteine residues (C271 and C321) in NSUN2 protein are essential for its proviral activity. NSUN2-KO or control A549 cells were transfected with pCAGGS-NSUN2 or mutants followed by infection with rgRSV (*F*, *G*, and *H*) or rVSV-GFP (*I*, *J*, and *K*) at an MOI of 1.0. Transfection of WT NSUN2 but not NSUN2-C271A or NSUN2-C321A rescued the GFP expression (*F* and *J*), viral titer (*G* and *K*), and viral protein expression (*H* and *I*) in NSUN2-KO cells. All results are from three independent experiments. Data were analyzed using s Student's *t* test (*$P < 0.05$; **$P < 0.01$).

m^{5}C Methyltransferase Activity of NSUN2 Is Required for Proviral Activity. Cytosine methylation by NSUN2 relies on two conserved cysteine residues (C271 and C321) (29). Alanine substitution of either of these two cysteine residues in NSUN2 abolishes its m^{5}C methyltransferase activity (29). We next evaluated whether the m^{5}C methyltransferase activity of NSUN2 is required for its proviral activity. Transfection of WT NSUN2 but not empty vector, NSUN2-C271A, or NSUN2-C321A rescued viral replication and gene expression of both RSV (Fig. 2 *F*–*H*) and VSV (Fig. 2 *I*–*K*), demonstrating that RNA m^{5}C methyltransferase of NSUN2 is essential for its proviral activity.

Antiviral Effect Mediated by NSUN2 Depletion Is Independent of Viral RNA m^{5}C Methylation. We next conducted the bisulfite-based m^{5}C sequencing to determine whether viral RNA contains m^{5}C and could be, therefore, regulated by NSUN2. Briefly, NSUN2-KO A549 cells and single-guide RNA (sgRNA) control A549 cells were infected with recombinant RSV expressing GFP (rgRSV) or rVSV-GFP at a multiplicity of infection (MOI) of 1.0, and total RNA was extracted from cells and subjected to bisulfite-based m^{5}C sequencing, which allows us to identify m^{5}C sites in viral RNAs and host RNAs. For neither virus did we observe any significant m^{5}C site by T>C mutation signature in positive-sense viral RNAs, which include both antigenome and mRNAs. As for the VSV genome, we did not observe any significant m^{5}C sites either. However, in RSV genome RNA, we discovered 20 notable m^{5}C sites with a T>C mutation ratio at 45 to 99% (Fig. 3*A*), spread in NS2, intergenic sequence (*IG*) between NS2 and N, P, *IG* between P and M, M, G, and M2 genes (Fig. 3*A*). Importantly, none of these m^{5}C sites was notably affected by NSUN2 depletion (Fig. 3*A* and *SI Appendix*, Fig. S3*A*). Collectively, antiviral effects mediated by NSUN2 depletion are independent of m^{5}C methylation in viral RNA.

Alteration of Host RNA m^{5}C Methylome by NSUN2 Depletion. We next analyzed whether NSUN2 regulates m^{5}C methylation of host RNAs. The bisulfite-based m^{5}C sequencing revealed 541 overlapped NSUN2-regulated m^{5}C sites in both RSV- and VSV-infected cells, which display over 20% T>C mutation ratio in WT and a significant reduction (>10%) of mutation ratio after NSUN2 KO (Fig. 3*B*). We identified 463 of 541 NSUN2-regulated m^{5}C sites located within cytoplasmic tRNAs (Fig. 3*C*), where NSUN2 is known to affect tRNA m^{5}C methylation (10, 30). Similar to the findings of previous research (11–13), we identified a number of NSUN2-regulated highly methylated m^{5}C sites in intergenic and intron regions (*SI Appendix*, Fig. S3 *B*–*D*). Among the abundant ncRNA, we identified an m^{5}C site in RPPH1 (ribonuclease P RNA component H1) (5) exhibiting a notably decreased methylation after NSUN2 depletion (Fig. 3*D*). In addition, we also confirmed the presence of NSUN2-regulated m^{5}C sites in snoRNA 62A/62B, small Cajal body–specific RNA (scaRNA)2, and vtRNA1-1 (Fig. 3 *E*–*G*). Since the m^{5}C methylome of host mRNAs was barely detectable based on m^{5}C-seq data from total cellular RNA, we built the m^{5}C-seq libraries with the purified polyadenylated RNA to enrich the mRNA fraction in order to generate deeper sequencing reads in mRNA regions. We detected a total of 47 confident, NSUN2-regulated m^{5}C sites, most of which are in the intergenic/intron regions and only three sites are within mRNA exons of NIBAN2, LXRB, and CDC37 using a stringent cutoff (*SI Appendix*, Fig. S3*E*). It should be noted that we also did not observe detectable m^{5}C sites in other mRNAs, particularly IFN-related genes such as type I, II, and III IFNs, IRF3, RIG-I, or

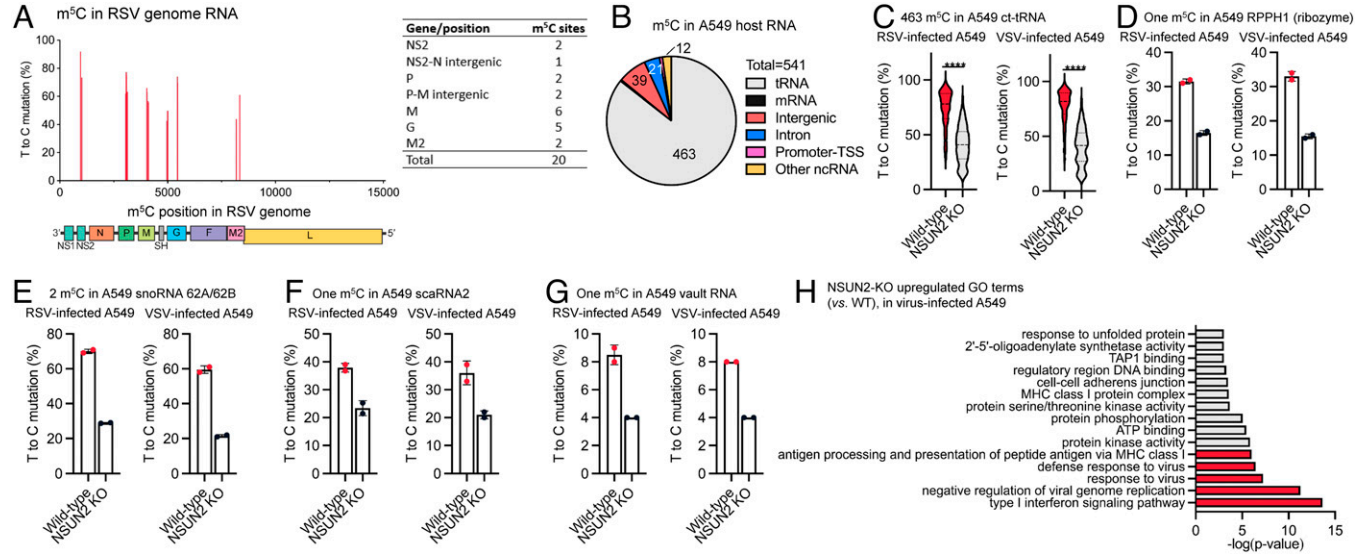

Fig. 3. NSUN2 depletion leads to an enhanced up-regulation of type I IFN signaling and antivirus immune response, in which it also controls the m^{5}C methylation in some A549 host RNAs. (*A*) (*Left*) location of 20 m^{5}C sites within RSV genome RNA. The *x* axis shows the m^{5}C site position in RSV genome; the *y* axis shows the m^{5}C site mutation level. (*Right*) Number of m^{5}C sites in each RSV gene. (*B*) Distribution of NSUN2-regulated m^{5}C sites in major RNA species from A549 host RNA (shared by both RSV-infected and VSV-infected cells). (*C*) Mutation levels of NSUN2-regulated m^{5}C sites in cytoplasmic tRNAs from NSUN2-KO A549 cells vs. WT cells. *P* values were determined using two-tailed *t* test for paired samples (****$P < 0.0001$). (*D*–*G*) Mutation levels of one m^{5}C site in RPPH1 (*D*), two m^{5}C sites in snoRNA 62A and 62B (*E*), one m^{5}C site in scaRNA2 (*F*), and one m^{5}C site in vault RNA (vtRNA1-1) (*G*) from NSUN2-KO A549 cells vs. WT cells. For (*D*)–(*G*), mean values ± SD are shown; $n = 2$. (*H*) Enriched GO clusters of up-regulated genes in virus-infected NSUN2-KO A549 cells (vs. virus-infected WT A549 cells). The clusters are ranked by *P* value.

MDA5 (*SI Appendix*, Fig. S3*E*), which is consistent with two previous observations (30, 31).

We also analyzed whether RSV and VSV infections alter host m^{5}C methylome in A549 cells. For the 447 m^{5}C sites in cytoplasmic tRNA, RSV and VSV infection significantly reduced the m^{5}C methylation level ($P < 0.0001$) (*SI Appendix*, Fig. S4*A*), suggesting that virus infection might impact host tRNA m^{5}C methylation and tRNA processing/biogenesis. We did not observe significant changes for m^{5}C sites on vtRNA1-1 with or without viral infection (*SI Appendix*, Fig. S4*B*). For the m^{5}C site in RPPH1 RNA, scaRNA2, and snoRNA62A, we observed a slight decrease in m^{5}C methylation in RSV- or VSV-infected cells (*SI Appendix*, Fig. S4 *C*–*E*).

m^{5}C-Mediated Antiviral Effect Is Driven by the Enhanced Type I IFN Response. To examine potential effects of m^{5}C depletion on host gene expression, we also constructed RNA sequencing (RNA-seq) libraries of total cellular RNA isolated from VSV-infected WT A549 or NSUN2-KO cells for Gene Ontology (GO) analysis. Notably, NSUN2-KO A549 cells displayed a significant up-regulation of gene clusters related to type I IFN signaling, negative regulation of viral genome replication, and defense response to virus infection, compared to the control sgRNA A549 cells (Fig. 3*H* and *SI Appendix*, Fig. S5). These observations prompted us to examine potential roles of innate immunity in inhibiting virus replication in NSUN2-depleted A549 cells.

To recapitulate the type I IFN signaling pathway, A549 cells were treated with control siRNA or siRNA against NSUN2 followed by infection with rgRSV (Fig. 4 *A* and *B*), hMPV (Fig. 4 *C* and *D*), or rVSV-GFP (Fig. 4 *E* and *F*), and RIG-I and MDA5 expression, IRF3 phosphorylation, and IFN-β were examined. Prior to virus infection, we detected significantly higher RIG-I and MDA5 expression, IRF3 phosphorylation (Fig. 4 *A*, *C*, and *E*), and IFN-β secretion (Fig. 4 *B*, *D*, and *F*) in siRNA against NSUN2 (siNSUN2)–treated A549 cells compared to the control siRNA-treated A549 cells. After virus infection, IFN-β dramatically increased in siNSUN2-treated A549 cells (Fig. 4 *B*, *D*, and *F*). Consistent with its antiviral role, viral protein synthesis was significantly reduced in NSUN2-knockdown cells (Fig. 4 *A*, *C*, and *E*). Similar results were also observed with NSUN2-KO cells and control sgRNA-transduced cells for RSV, VSV, and hMPV infection (*SI Appendix*, Fig. S6 *A*–*E*).

To determine whether the enhanced type I IFN response is dependent on viral replication, we transfected cells with viral genome RNA isolated from virions or polyinosinic-polycytidylic acid [poly(I:C)]. These single-stranded virion RNAs are triphosphorylated and known to be the ligand for RIG-I. Equal amounts of virion RNA were transfected into WT A549 cells and NSUN2-KO cells. Under these conditions, there would be no viral replication. However, similar to virus infection, RIG-I and MDA5 expression and IRF3 phosphorylation in cell lysates and IFN-β secretion were significantly increased in NSUN2-KO cells compared to the control sgRNA-transduced A549 cells for RSV (Fig. 4 *G* and *H*), hMPV (Fig. 4 *I* and *J*), and VSV (Fig. 4 *K* and *L*) virion RNA. We realized that the IFN-β was near the detection limit by ELISA-based IFN-β assay in NSUN2-KO A549 cells prior to virus infection. Thus, we used more sensitive real-time RT-PCR to quantify IFN-α and IFN-β mRNAs. As expected, both IFN-α and IFN-β mRNAs were significantly increased in NSUN2-KO A549 cells compared to the control sgRNA-treated A549 cells (Fig. 4*M*), which was consistent with the enhanced RIG-I and MDA5 expression prior to virus infection (Fig. 4 *G*, *I*, and *K*). Thus, the innate immune system has been activated in A549 cells upon depletion of NSUN2 cells. Enhanced RIG-I, MDA5, and IFN-β were also observed in siNSUN2-treated A549 cells transfected with RSV, hMPV, and VSV virion RNA (*SI Appendix*, Fig. S6 *F*–*J*). Similarly, IFN-β was significantly increased in siNSUN2-treated A549 cells transfected with poly(I:C), an analog of double-stranded RNA (dsRNA), known to induce a type I IFN response (Fig. 4*N*). Also, IFN-β was significantly increased in siNSUN2-treated A549 cells upon infection with recombinant Sendai virus (rSeV)-GFP

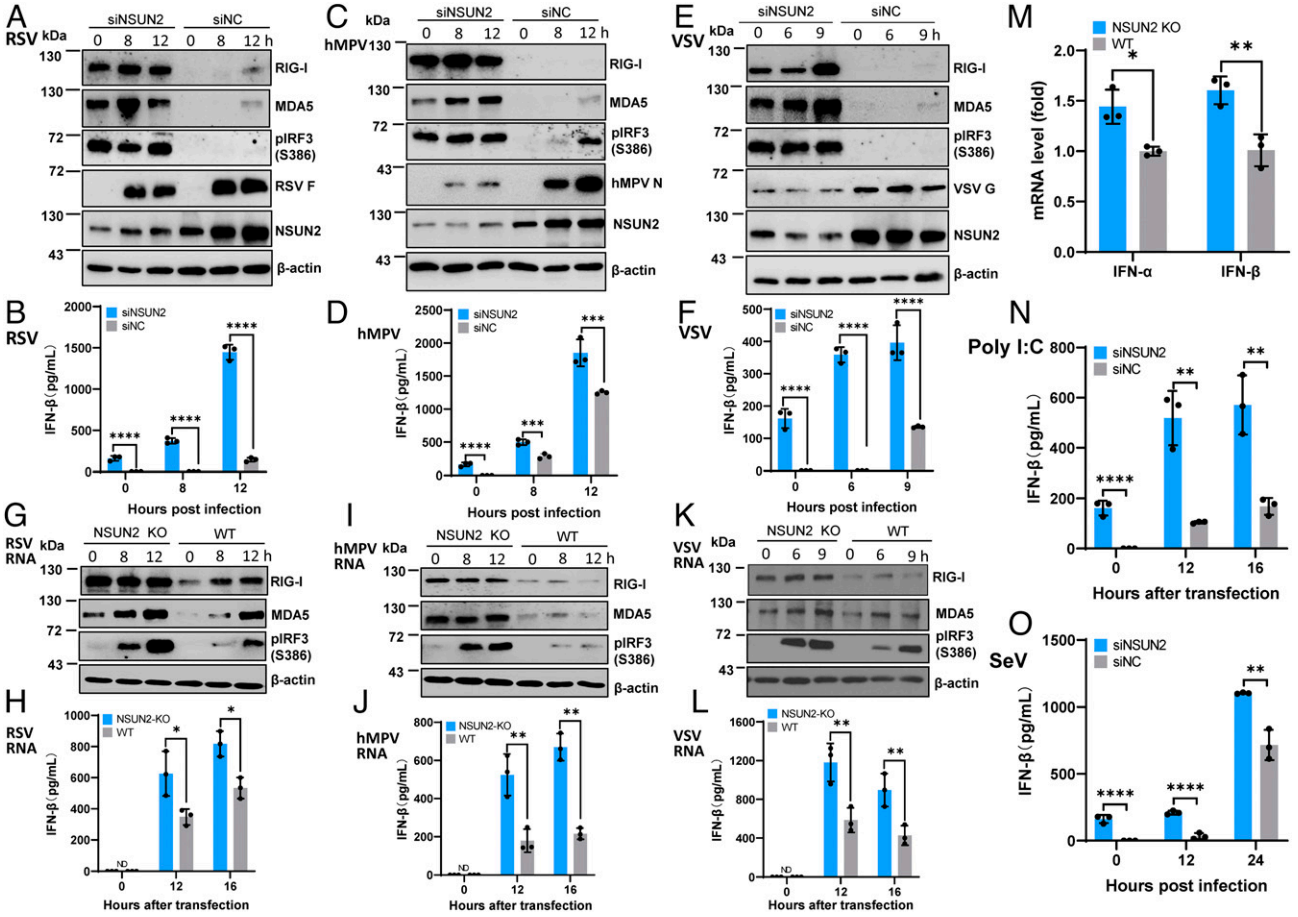

Fig. 4. NSUN2 depletion leads to the activation of a higher type I IFN signaling pathway. (*A–F*) NSUN2 depletion induces a higher type I IFN after virus infection. A549 cells were transfected with siNSUN2 or siNC, and were infected with rgRSV (*A* and *B*), hMPV (*C* and *D*), or rVSV-GFP (*E* and *F*) at an MOI of 1.0, 5.0, and 1.0, respectively. Cell lysates were subjected to Western blot analyses (*A*, *C*, and *E*). IFN-β in cell culture supernatants was detected by ELISA (*B*, *D*, and *F*). (*G–L*) NSUN2 KO induces a higher type I IFN after transfection with viral RNA. NSUN2-KO or control A549 cells were transfected with virion RNAs (2×10^6 copies/well) of rgRSV (*G* and *H*), hMPV (*I* and *J*), or rVSV-GFP (*K* and *L*). ND indicates the value was below the detection limit (50 pg/mL). (*M*) Quantification of IFN mRNA by RT-qPCR. Total RNA was extracted from NSUN2-KO or control sgRNA-treated A549 cells. IFN-α and IFN-β mRNA was quantified by RT-qPCR. β-actin was used for internal control. (*N*) NSUN2 KO induces a higher type I IFN after transfection with poly(I:C). Cells were transfected with 0.5 μg/well of poly(I:C). (*O*) NSUN2 KO induces a higher type I IFN after infection with rSeV-GFP. An MOI of 1.0 was used for infection. Data were analyzed using a Student's *t* test (*$P < 0.05$, **$P < 0.01$, ***$P < 0.001$, ****$P < 0.0001$).

(Fig. 4*O*). Therefore, the m^5C deficiency-mediated antiviral effect is driven by the enhanced type I IFN responses, and this mechanism appears to be universally conserved in response to stimulants [such as virus infection, viral RNA, and poly(I:C)].

m^5C Deficiency-Mediated Antiviral Response Is Dependent on RIG-I but Not MDA5. To identify which RNA sensors are involved in the activation of type I IFN signaling, we examined viral replication and gene expression in A549 cells lacking RIG-I or MDA5 followed by NSUN2 depletion. Briefly, RIG-I-KO A549 cells (A549-RIG-$I^{-/-}$) and WT A549 cells were transfected with siRNA against NSUN2 or control siRNA, followed by infection with rgRSV. Consistently, knockdown of NSUN2 in WT A549 cells led to a significant reduction in RSV replication (Fig. 5 *A* and *B*). Remarkably, GFP expression (Fig. 5*A*), viral protein expression (*SI Appendix*, Fig. S7*A*), and RSV titer (Fig. 5*B*) were completely restored in A549-RIG-$I^{-/-}$ cells when NSUN2 was depleted. Thus, the NSUN2 deficiency-mediated antiviral response is dependent on RIG-I. Next, we used two rounds of siRNA transfection to knock down MDA5 and NSUN2 in WT A549 cells (*SI Appendix*, Fig.7 *B* and *C*), followed by rgRSV infection. Viral replication was not restored in A549 cells when both MDA5 and NSUN2 were depleted (Fig. 5*C* and *SI Appendix*, Fig. S7*C*). Therefore, MDA5 does not play a significant role in antiviral response mediated by NSUN2 depletion.

RIG-I Recognizes Host ncRNAs That Are Regulated by NSUN2. We next utilized RIP-seq to identify which RNA species containing NSUN2-regulated m^5C sites are recognized by RIG-I. We purified the RNAs that immunoprecipitated together with FLAG-tagged RIG-I (FLAG-RIG-I) in transfected control sgRNA-transduced and NSUN2-KO A549 cells that had been infected with rgRSV or rVSV-GFP, followed by deep sequencing the IP-enriched RNAs. In control sgRNA-transduced A549 cells, by comparing the overlapping targets between RSV and VSV infections (Fig. 6 *A* and *B*), 7SL RNA (or RN7SL) including 7SL1, 7SL2, and 7SL3 appeared as the top enriched candidates in RIG-I IP, together with 7SL RNA pseudogenes (7SL5P and 7SL4P). In NSUN2-depleted cells (Fig. 6 *C* and *D*), we observed consistent top targets of RIG-I such as 7SL RNA, 7SK RNA, and RPPH1. Most of these RIG-I–bound RNAs are ncRNAs, which are transcribed through RNA polymerase III (Pol III) (32, 33).

We next performed RNA-seq to verify effects of NSUN2 depletion on RNA levels of Pol III–transcribed RNA species. NSUN2 KO led to significant increases in RNA levels of 7SL (Fig. 6*E*) and 7SK RNA (Fig. 6*F*), all of which are the signal

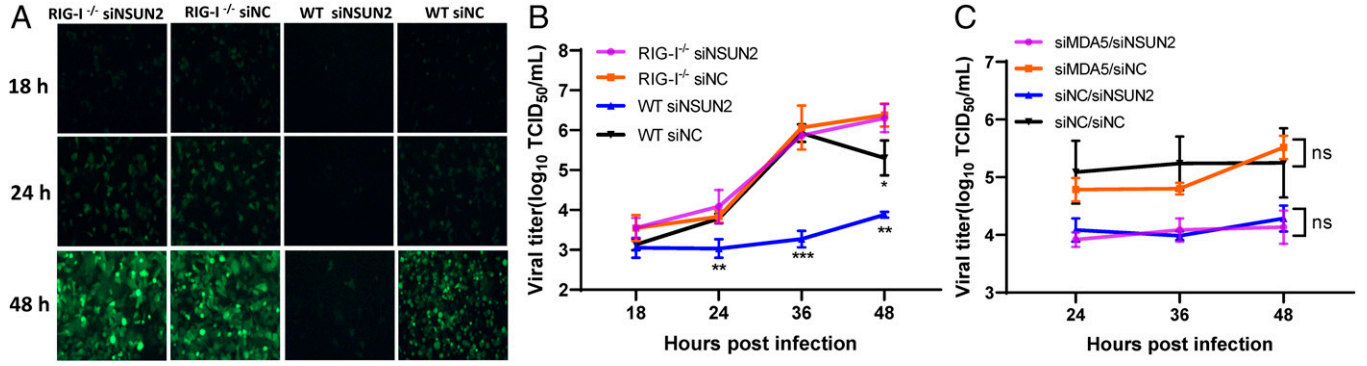

Fig. 5. m^{5}C deficiency-mediated antiviral response is dependent on RIG-I but not MDA5. Confluent WT A549 cells and RIG-I-KO (RIG-I$^{-/-}$) A549 cells were transfected with siRNA against NSUN2 or control siRNA, followed by infection with rgRSV at an MOI of 0.1. GFP images were taken by fluorescence microscopy (*A*) and viral titer in cell culture supernatants was determined by a 50% tissue culture infective dose ($TCID_{50}$) (*B*). (*C*) A549 cells were transfected with siRNA against NSUN2, MDA5, or both, followed by infection with rgRSV at an MOI of 0.1, and viral titer in cell culture supernatants was determined by $TCID_{50}$. Data were analyzed using a Student's *t* test (*$P < 0.05$, **$P < 0.01$, ***$P < 0.001$).

recognition particle (SRP) RNAs. Elevated levels in other Pol III–transcribed RNAs such as RPPH1 (Fig. 6*G*) and Y RNAs (Fig. 6*H*) were observed in NSUN2-depleted cells as well, whereas these effects were not obvious for the 5S rRNA pseudogenes and vtRNAs (*SI Appendix*, Fig. S8 *A* and *B*). Because 7SL RNA is one of the most abundant RNAs inside cells, the elevation in its RNA level, under NSUN2 depletion, might yield a large amount of unshielded 7SL RNAs, which is known to trigger a RIG-I response (34).

Since many ncRNAs form a dsRNA structure, we next conducted IP of dsRNA using the dsRNA-specific antibody and performed sequencing of the enriched dsRNA. NSUN2 depletion leads to more than threefold increases in RNA abundance of more than 25 genes after dsRNA-IP (*SI Appendix*, Fig. S8*C*), especially with 7SL and 7SK RNA enriched by 4- to 10-fold.

NSUN2 Depletion Enhances Transcription but Not Stability of ncRNAs. We hypothesized that NSUN2 depletion may enhance transcription and/or stability of ncRNAs thereby increasing ncRNA levels in cells. To analyze the transcription activity, NSUN2-KO and WT A549 cells were metabolically labeled with 5-ethynyl uridine (EU) which detects the transcription rate of the nascent RNA. The kinetics of RPPH1, 7SL, and 7SK RNA transcription was quantified by RT-qPCR. The transcription rate of all of these RNA species was significantly enhanced in NSUN2-KO cells compared to the WT cells (*SI Appendix*, Fig. S9 *A–C*). Similar results were observed in A549 cells transfected with siRNA targeting NSUN2 (*SI Appendix*, Fig. S9 *D–F*). To analyze the stability of ncRNAs, NSUN2-KO and WT A549 cells were treated with Pol III transcription inhibitor ML-60218 and the kinetics of ncRNA decay were quantified by RT-qPCR. No significant difference in decay

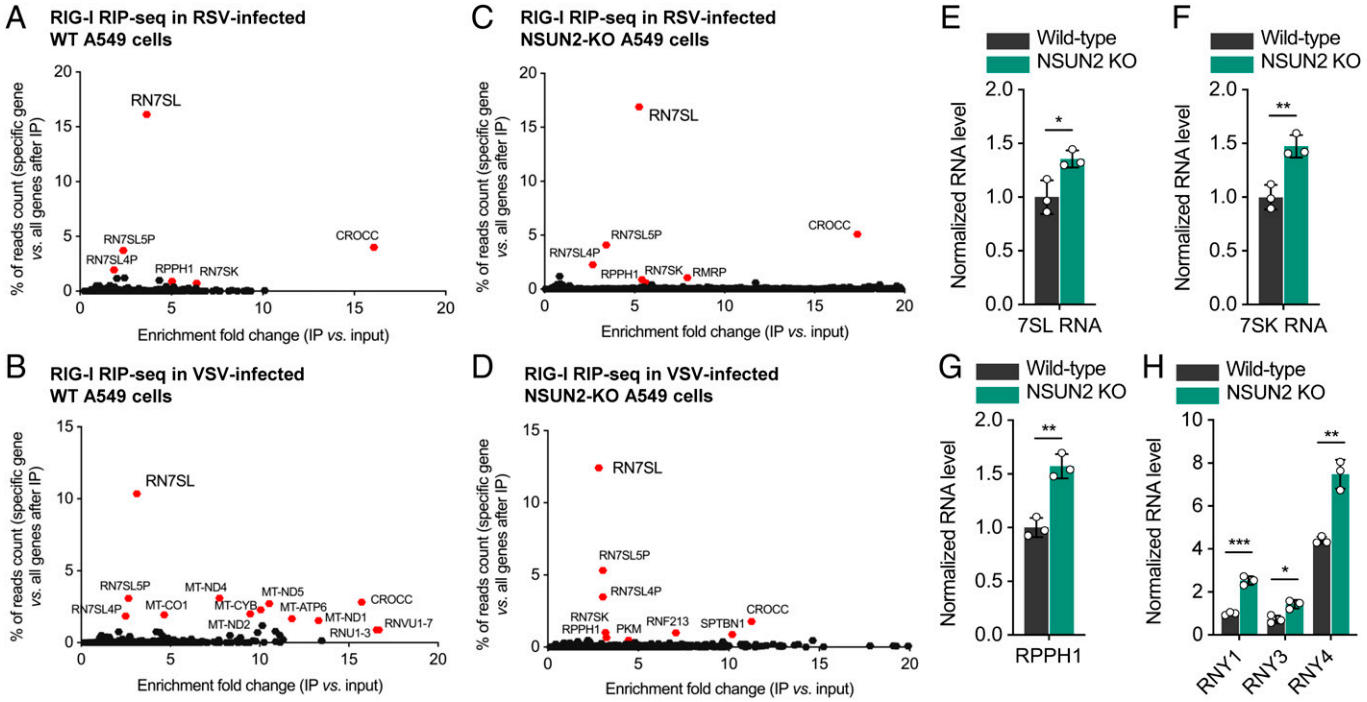

Fig. 6. RIG-I binds to 7SL RNA (RN7SL) in vivo when overexpressing RIG-I in A549 cells, and NSUN2 depletion leads to elevated Pol III transcription of 7SL, 7SK, RPPH1, and Y RNA. Enriched genes in RIG-I RIP-seq when overexpressing RIG-I in RSV (*A*)- or VSV (*B*)-infected WT A549 cells. Enriched genes in RIG-I RIP-seq when overexpressing RIG-I in RSV (*C*)- or VSV (*D*)-infected NSUN2-KO A549 cells. For (*A*)–(*D*), the *y* axis shows the percentage of how much the reads count from one specific gene occupies in all IP-enriched genes; the *x* axis shows the enrichment fold change after IP (vs. input). (*E–H*) Relative RNA levels of 7SL (*E*), 7SK (*F*), RPPH1 (*G*), and Y (*H*) RNAs in NSUN2-KO A549 cells vs. the WT A549 cells without viral infection, which are transcribed by Pol III. For (*E*)–(*H*), mean values ± SD are shown; $n = 3$ biologically independent samples. *P* values were determined using an unpaired *t* test (*$P < 0.05$, **$P < 0.01$, ***$P < 0.001$).

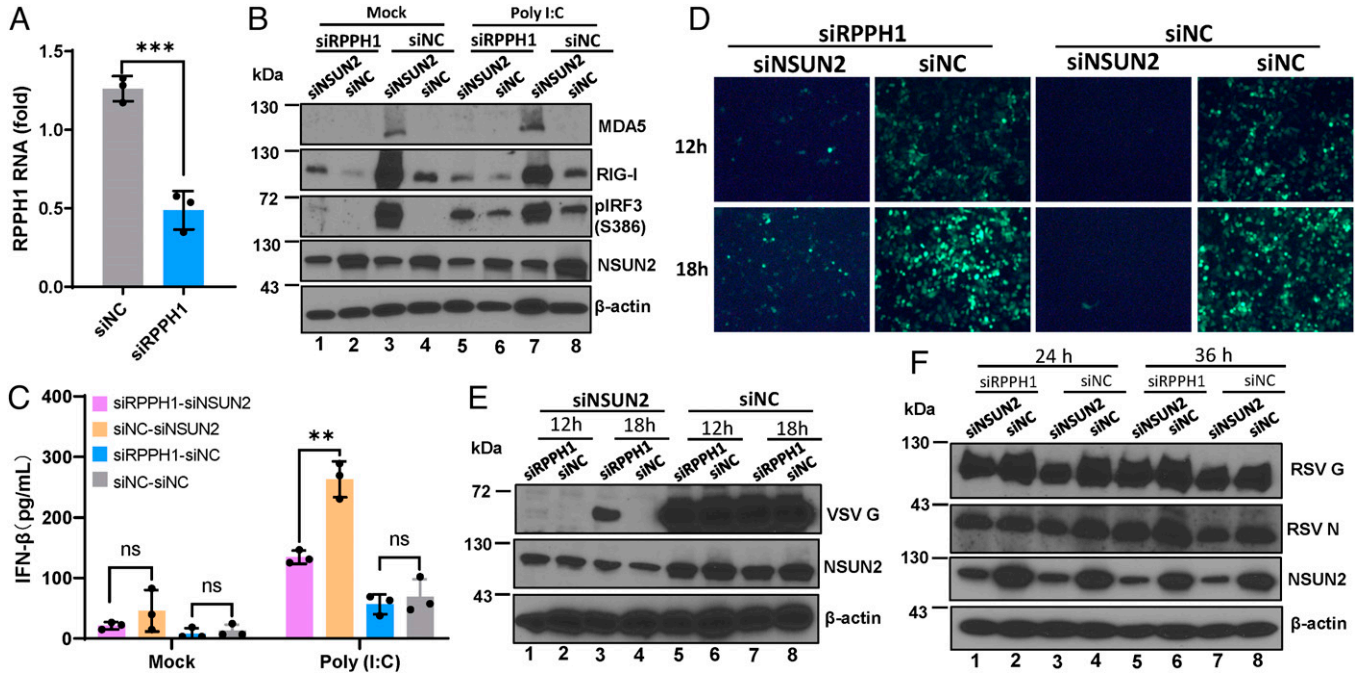

Fig. 7. Silencing of RPPH1 rescues virus replication. (*A*) Knockdown of RPPH1 by siRNA. A549 cells were transfected with control siRNA or siRNA against RPPH1, and RPPH1 RNA was quantified by RT-qPCR. (*B* and *C*) Silencing of RPPH1 attenuates IFN signaling. A549 cell were transfected with siNSUN2/siRPPH1, siNSUN2/siNC, siRPPH1/siNC, or siNC, followed by transfection with poly(I:C), and cell lysate and supernatant were harvested for Western blot (*B*) and ELISA (*C*) at 0 and 8 h after transfection. (*D*–*F*) Silencing of RPPH1 partially rescues VSV and RSV replication. A549 cells were treated with siRNAs described in (*B*), followed by infection with rVSV-GFP (*D* and *E*) and rgRSV (*F*) at an MOI of 0.1; representative GFP images in rVSV-GFP–infected cells were monitored (*D*). Cell lysates were prepared for Western blot against VSV (*E*) or RSV (*F*) proteins. Data were analyzed using Student's *t* test (**$P < 0.01$, ***$P < 0.001$).

kinetics was observed for RPPH1, 7SL, and 7SK RNAs between NSUN2-KO and WT A549 cells (*SI Appendix*, Fig. S10), suggesting that NSUN2 KO may not affect the stability of ncRNAs.

Inhibition of ncRNA Transcription and Silencing RPPH1 Attenuate the IFN Response That Partially Rescues Viral Replication. It is known that RPPH1 facilitates Pol III transcription of diverse small RNAs and long ncRNAs (lncRNAs), including tRNA, 5S rRNA, 7SL RNA, and U6 snRNA genes (32, 35, 36). Thus, we hypothesized that the NSUN2-altered m^5C methylation of RPPH1 RNA might impact RNase P enzymatic activity or levels which are essential for Pol III transcription. To test this hypothesis, we first used ML-60218, an RNA Pol III inhibitor, to directly inhibit Pol III transcription (37). As a positive control, after stimulating with poly(I:C), treatment of NSUN2-depleted A549 cells with ML-60218 led to suppression of RIG-I and MDA5 expression, IRF3 phosphorylation (*SI Appendix*, Fig. S11 *A* and *B*), and IFN-β secretion (*SI Appendix*, Fig. S11*C*) in a dose-dependent manner compared to the NSUN2-depleted A549 cells treated with dimethyl sulfoxide (DMSO) control. Importantly, VSV protein expression (*SI Appendix*, Fig. S11*D*), GFP signal (*SI Appendix*, Fig. S11 *F* and *H*), and VSV titer (*SI Appendix*, Fig. S11 *E* and *G*) were partially restored in NSUN2-depleted A549 cells treated with ML-60218 in a dose-dependent manner whereas VSV replication was not significantly changed in control A549 cells treated with ML-60218. Similarly, RSV protein expression (*SI Appendix*, Fig. S12 *A* and *D* [compare lanes 1 and 3, 5 and 7]), GFP expression (*SI Appendix*, Fig. S12*C*), and viral titer (*SI Appendix*, Fig. S12 *B* and *E*) were partially rescued in NSUN2-depleted A549 cells treated with increasing doses of ML-60218.

As a second approach, we sought to knock down RPPH1 using siRNA (Fig. 7*A*). As a positive control, upon stimulation with poly(I:C), knockdown of RPPH1 led to the suppression of RIG-I and MDA5 expression, IRF3 phosphorylation (Fig. 7*B*), and IFN-β secretion (Fig. 7*C*) in NSUN2-depleted cells compared to the control siRNA-treated cells. Similarly, VSV (Fig. 7 *D* and *E*, compare lanes 1 and 3) and RSV (Fig. 7*F*, compare lanes 1 and 3, 5 and 7) replication and protein expression were partially restored in NSUN2-depeleted A549 cells when RPPH1 was knocked down. Collectively, these results demonstrate that suppression of ncRNA transcription and silencing RPPH1 attenuate IFN signaling and partially rescue viral replication in NSUN2-depeleted cells.

NSUN2 Depletion Leads to an Increased Level of Unshielded 7SL RNA. We next determined the role of 7SL RNA in IFN signaling, as they are the top up-regulated hits upon NSUN2 depletion even though they are already highly abundant in cells at steady state. 7SL RNA typically forms complexes with SRP proteins. We hypothesized that an increase in 7SL RNA level will lead to the accumulation of unshielded 7SL RNA that activates RIG-I. We first confirmed that 7SL RNA had ∼2.5-fold increases in siNSUN2-treated A549 cells compared to control siRNA-treated cells, as quantified by real-time qPCR (Fig. 8*A*). We then treated cells with micrococcal nuclease (MNase) with or without membrane permeabilization followed by real-time qPCR to quantify shielded and unshielded 7SL RNA (Fig. 8*B*). This experiment revealed a significant increase in unshielded 7SL RNA in NSUN2 knockdown cells compared to the control siRNA-treated A549 cells (Fig. 8*B*).

Two SRP proteins, SRP9 and SRP14, normally bind the 5′ end of 7SL RNA and shield 7SL RNA from being recognized by RIG-I (38). We hypothesized that overexpression of SRP9 and SRP14 will bind to the unshielded 7SL RNA in NSUN2-KO cells, thereby rescuing the phenotype. Briefly, NSUN2-KO or WT A549 cells were transfected with empty vector or plasmid encoding SRP9 or SRP14, followed by infection with

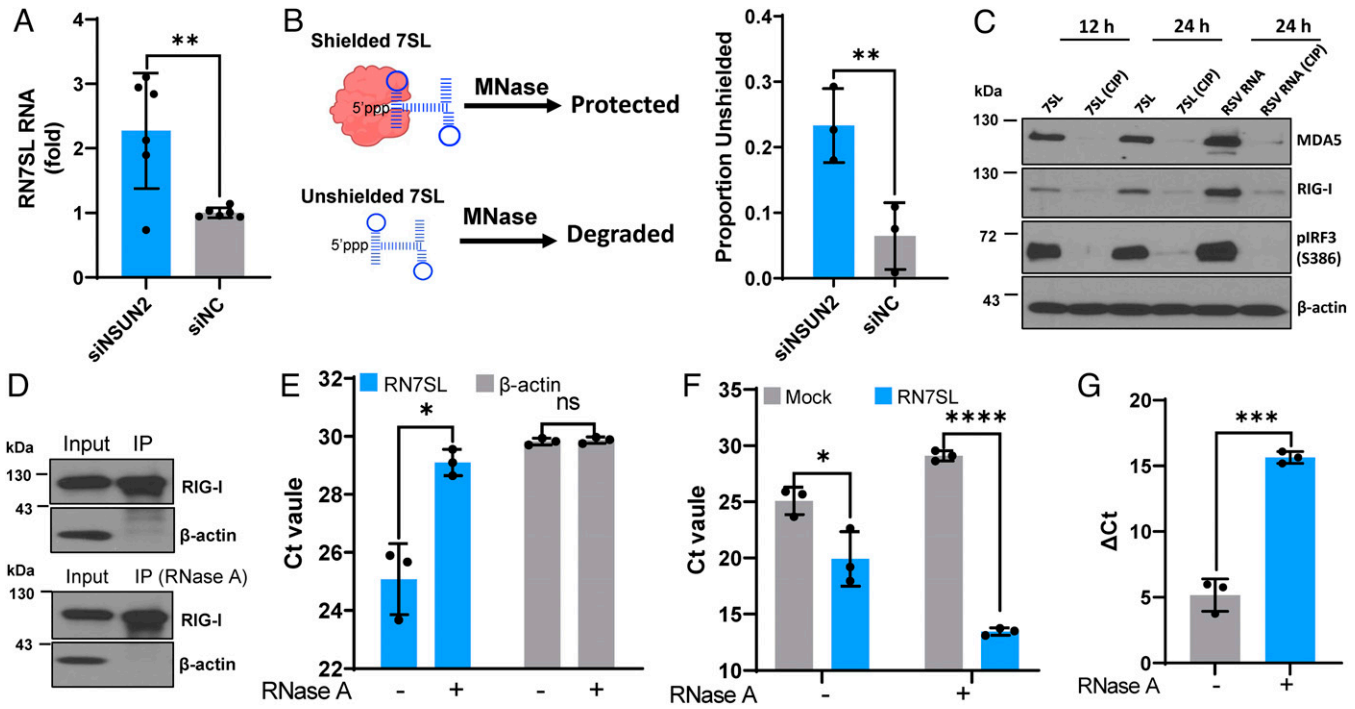

Fig. 8. 7SL RNAs are the direct ligands of RIG-I. (*A*) Total 7SL RNAs are elevated in NSUN2 knockdown cells. A549 cells were transfected with siNSUN2 or siNC. At 24 h posttransfection, 7SL RNA was quantified by RT-qPCR and normalized by β-actin mRNA. Data shown are fold increases in NSUN2-depleted cells relative to the control siRNA-treated cells. (*B*) Unshielded 7SL RNAs are elevated in NSUN2 knockdown cells. A549 cells were transfected with siNSUN2 or siNC, incubated with or without MNase, and the unshielded 7SL RNAs were measured by RT-qPCR. The 7SL RNAs were normalized by β-actin mRNA. Data shown are unshielded 7SL RNA relative to total 7SL RNA. (*C*) 7SL RNAs activate RIG-I signaling. A549 cells were transfected with in vitro–transcribed 7SL RNA or RSV virion RNA pretreated with or without CIP. The cell lysates were harvested for Western blot. (*D*–*G*) Pulldown of 7SL RNA by RIG-I. HEK293T cells were transfected with FLAG–RIG-I plasmid, and the input and immunoprecipitated RIG-I proteins were analyzed by Western blot (*D*). The purified FLAG–RIG-I proteins were treated with or without RNase A to remove endogenous 7SL RNA (*E*). The purified FLAG–RIG-I proteins with or without RNase A treatment were inoculated with or without in vitro–transcribed 7SL RNA, and the level of 7SL RNA bound to RIG-I was measured by RT-qPCR (*F* and *G*). Data are presented as cycle threshold (Ct) (*F*) and ΔCt (ΔCt = $Ct_{Mock} - Ct_{7SL}$) (*G*). All data are from three ($n = 3$) independent experiments (except *A*, $n = 6$). Data were analyzed using a Student's *t* test (*$P < 0.05$, **$P < 0.01$, ***$P < 0.001$, ****$P < 0.0001$).

rVSV-GFP. Overexpression of SRP9 or SRP14 partially rescued VSV replication, protein synthesis, and viral titer in NSUN2-KO cells (*SI Appendix*, Fig. S13). These results suggest that the unshielded 7SL levels increased in NSUN2-KO cells are bound and shielded by the overexpressed SRP9 and SRP14 proteins, thereby rescuing viral replication.

7SL RNAs Are Direct Ligands of RIG-I. To demonstrate that 7SL RNAs can be directly detected by RIG-I, we synthesized 7SL RNAs in vitro and characterized their interaction with RIG-I. Similar to triphosphorylated RSV virion RNA, transfection of 7SL RNAs into A549 cells triggered a high level of RIG-I, MDA5, and IRF3 phosphorylation (Fig. 8*C*). Treatment of 7SL and RSV virion RNAs by alkaline calf intestinal phosphatase (CIP), which removes 5′ phosphorylated ends of RNA, abolished IFN signaling (Fig. 8*C*). Next, we determined whether in vitro–synthesized 7SL RNAs can directly bind to FLAG-tagged RIG-I purified from HEK-293T cells. The purified FLAG-tagged RIG-I was conjugated to magnetic beads (Fig. 8*D*), followed by treatment with RNase A to remove any RNA that has been bound to RIG-I. RNase A treatment led to a significant reduction in 7SL RNA, suggesting that 7SL RNA was copurified with RIG-I (Fig. 8*E*). As a control, no significant reduction was observed for β-actin mRNA with or without RNase treatment (both were at the detection limit level) (Fig. 8*E*). Next, the FLAG-tagged RIG-I (either with or without RNase A) was mixed with the in vitro–synthesized 7SL RNA, pulled down with FLAG antibody, and the RNA in the complex was quantified by RT-qPCR. Significant amounts of 7SL RNAs were bound to RIG-I (Fig. 8 *F* and *G*). As expected, RNase A–treated RIG-I (free of 7SL RNA) has more 7SL RNA bound compared to the untreated RIG-I (Fig. 8 *F* and *G*), demonstrating that 7SL RNA binds efficiently to RIG-I. Thus, these results indicate that 7SL RNAs are direct ligands of RIG-I.

Silencing of 7SL RNAs Attenuates IFN Signaling and Rescues Viral Replication. To further characterize the role of 7SL RNA, we knocked down 7SL RNA in WT and NSUN2-knockdown A549 cells and examined the IFN response and viral replication. We confirmed that 7SL RNA can be efficiently reduced by siRNA knockdown (Fig. 9*A*). Upon stimulation by poly(I:C), RIG-I and MDA5 expression, IRF3 phosphorylation, and IFN-β secretion were strongly suppressed in 7SL RNA and NSUN2 double knockdown A549 cells compared to NSUN2 knockdown A549 cells alone (Fig. 9 *B* and *C*). Notably, upon infection with rVSV-GFP, GFP signal (Fig. 9*D*), VSV G protein expression (Fig. 9 *E* and *F*), and VSV titer (Fig. 9*G*) were remarkably rescued when 7SL RNA was knocked down in NSUN2-depleted A549 cells. This effect was attributed to the reduced IFN responses because RIG-I, MDA5, and IRF3 phosphorylation were significantly reduced upon 7SL RNA knockdown (Fig. 9*E*). Similar restoration of viral protein expression was observed for RSV when 7SL was knocked down (Fig. 9*H*). Thus, these results demonstrate that knockdown of 7SL RNA, the ligand for RIG-I, attenuates the IFN responses in NSUN2-depleted cells that significantly restore viral replication and gene expression.

Knockdown of NSUN2 in Human Bronchial Epithelial (HBE) Culture, an Ex Vivo Lung Airway Model, Enhances the Innate Immune Response and Reduces RSV Replication. We also examined the effects of NSUN2 knockdown on RSV innate

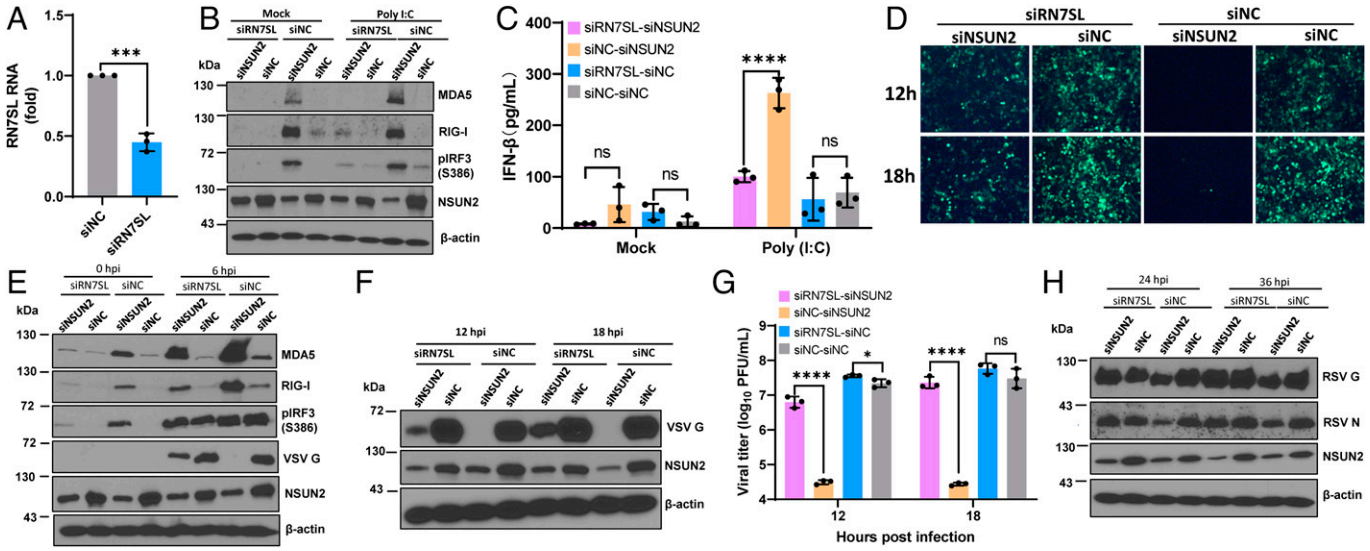

Fig. 9. Silencing of 7SL RNA (RN7SL) rescues virus replication. (*A*) Efficient knockdown of 7SL RNA using siRNA. A549 cells were transfected with siRNA against 7SL or control siRNA. At 24 h later, 7SL RNA was quantified by RT-qPCR. (*B* and *C*) Silencing of 7SL RNA attenuates IFN signaling upon poly(I:C) stimulation. A549 cells were transfected with siNSUN2/si7SL, siNSUN2/siNC, si7SL/siNC, or siNC, followed by transfection with poly(I:C), and cell lysates were harvested for Western blot (*B*) and supernatants were collected for measurement of IFN-β by ELISA (*C*) at 0 and 8 h after transfection. (*D*–*G*) Silencing of 7SL RNA partially rescues VSV replication. A549 cells were transfected with siNSUN2/si7SL, siNSUN2/siNC, si7SL/siNC, or siNC, followed by infection with rVSV-GFP at an MOI of 0.1. GFP images were taken by fluorescence microscopy (*D*). At early (0 and 6 h) (*E*) and late (12 and 18 h) (*F*) time points after infection, cell lysates were harvested for Western blot. VSV titer was rescued in NSUN2 and 7SL double-silenced A549 cells (*G*). (*H*) Silencing of 7SL RNA partially rescues RSV replication. A549 cells were treated with siRNA described in (*D*) and infected with rgRSV at an MOI of 0.1; cell lysates were subjected to Western blot. All data are from three ($n = 3$) independent experiments. Data were analyzed using a Student's *t* test (*$P < 0.05$, ***$P < 0.001$, ****$P < 0.0001$).

immune responses and replication in well-differentiated primary HBE cultures, a "near in vivo" human lung model for RSV infection (39, 40). We used a CRISPR-Cas9 technique to knock down NSUN2 in HBE culture (*SI Appendix*, Fig. S14 *A* and *B*). Following infection with rgRSV, a significantly less GFP-positive signal was observed in NSUN2-depleted HBE culture (*SI Appendix*, Fig. S14*C*). Quantification by ImageJ showed that NSUN2-depleted HBE culture had significantly less mean fluorescence intensity (MFI) compared to the control sgRNA-treated HBE culture at days 2 and 3 postinfection ($P < 0.01$ or 0.05) (*SI Appendix*, Fig. S14*D*). Furthermore, viral titer released from the apical surface of NSUN2-depleted HBE culture was significantly lower than that released from control sgRNA-treated HBE culture at days 1 to 3 ($P < 0.05$) (*SI Appendix*, Fig. S14*E*).

We next determined whether the reduced RSV replication and gene expression in NSUN2-depleted HBE culture was due to the enhanced innate immune response. We are particularly interested in those cytokines involved in IFN responses, which include IFN-α and IFN-β (type I IFN), IFN-λ1, -2, and -3 (type III IFN), IFN-γ (type II IFN), and IP-10. For this purpose, apical and basolateral fluids were collected at day 3 postinoculation for cytokine detection. NSUN2 depletion led to a significant increase in type I, II, and III IFN responses in both apical and/or basolateral fluids compared to the control sgRNA-treated HBE (*SI Appendix*, Fig. S14 *F*–*K*). Thus, depletion of NSUN2 in HBE culture leads to enhanced innate immune responses which in turn inhibit RSV replication.

KO of NSUN2 in Mice Reduces Viral Replication and Pathology Accompanied with Enhanced Type I IFN Responses. We next determined whether NSUN2-mediated regulation of antiviral innate immunity occurred in vivo in a mouse model. Briefly, 4-6-wk-old WT ($NSUN2^{+/+}$) mice and $NSUN2^{+/-}$ mice (11, 41) were intranasally inoculated with RSV or VSV, and were euthanized at day 3 postinfection. RSV genome replication was significantly reduced in lungs from $NSUN2^{+/-}$ mice ($P < 0.01$) compared to the lungs from WT mice (Fig. 10*A*), although there was no significant difference in RSV RNA replication in the nasal turbinates between these two groups ($P > 0.05$) (Fig. 10*B*). Importantly, both IFN-α and IFN-β mRNA expression significantly increased in $NSUN2^{+/-}$ mice compared to the control WT mice (Fig. 10*C*). For WT mice, RSV infection induced moderate to severe lung histological changes, including interstitial pneumonia, bronchiolitis, and inflammation in lungs (Fig. 10 *D* and *E* and *SI Appendix*, Fig. S15*A*). However, significantly less lung pathology was observed in lungs from $NSUN2^{+/-}$ mice (Fig. 10 *D* and *E*) ($P < 0.05$). Thus, NSUN2 KO leads to the enhanced type I IFN responses which suppress RSV replication in the lungs of mice.

Similar results were observed for VSV infection in $NSUN2^{+/-}$ and WT mice. VSV titer was significantly reduced in lungs from the $NSUN2^{+/-}$ mice (Fig. 10*F*) ($P < 0.05$), which was accompanied by a significant increase in both IFN-α and IFN-β mRNA (Fig. 10*K*) ($P < 0.001$). VSV infection in WT mice displayed moderate to severe pneumonia in the lungs whereas lungs from the $NSUN2^{+/-}$ mice had only mild lung histological changes (Fig. 10 *G* and *H* and *SI Appendix*, Fig. S15*B*). Intranasal inoculation of VSV mice can lead to brain infection. VSV titer in brains was significantly reduced in $NSUN2^{+/-}$ mice (Fig. 10*I*) ($P < 0.05$). The brain tissue from VSV-infected WT mice had mild encephalitis (*SI Appendix*, Fig. S16). In contrast, the brain tissue from the $NSUN2^{+/-}$ mice had no signs of encephalitis (*SI Appendix*, Fig. S16). These results illustrate that NSUN2 deficiency in vivo is accompanied by an increased abundance of type I IFN which in turn suppresses viral replication and reduces viral pathogenesis.

Inhibition of NSUN2 by Peptide-Conjugated Phosphorodiamidate Morpholino Oligomer (PPMO) Diminishes Viral Replication and Pathogenesis. Finally, we determined whether NSUN2 can be used as a target for antiviral therapy in vivo. For this

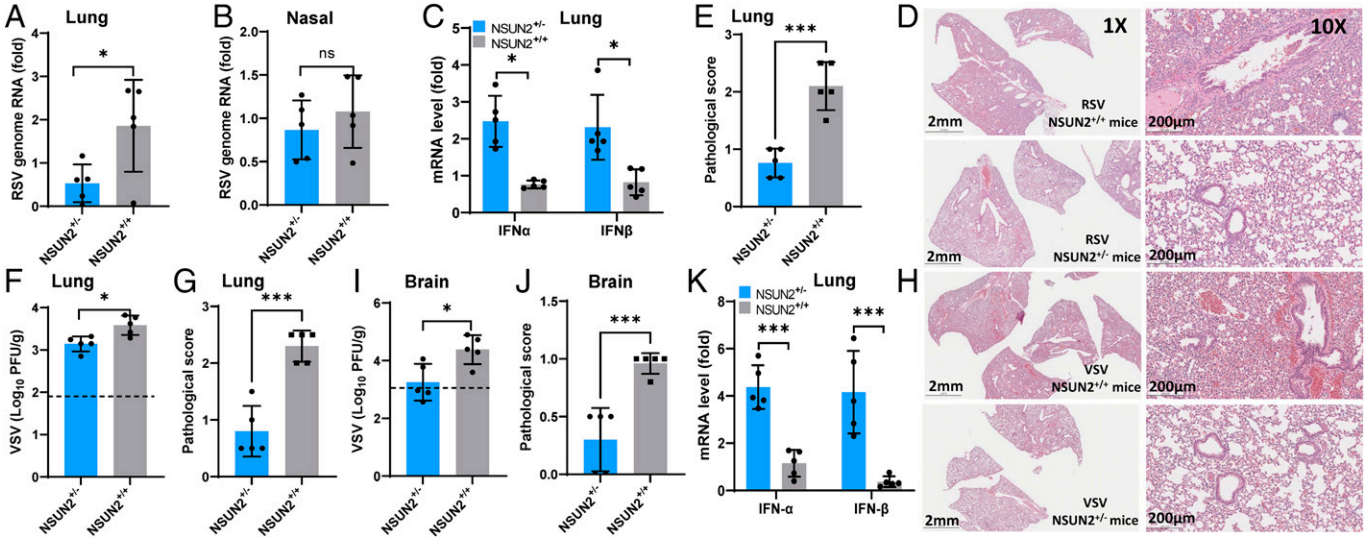

Fig. 10. Knockout of NSUN2 in mice reduces viral replication and enhances type I IFN responses. (*A–E*) RSV infection in NSUN2$^{+/-}$ and WT (NSUN2$^{+/+}$) mice. The 4-6-wk-old specific pathogen-free (SPF) female WT mice and NSUN2$^{+/-}$ mice were intranasally inoculated with 4×10^5 $TCID_{50}$ of rgRSV. At day 3 postinoculation, mice were euthanized and total RNA was extracted from the right lung (*A*) and the nasal turbinate (*B*) from each mouse for quantification of RSV genome RNA and type I IFN (IFN-α and IFN-β) mRNA in lungs (*C*) by real-time RT-PCR. Representative lung histological images (*D*) and average lung histology score from each group are shown (*E*). Each slide was scored based on severity of lesion. Scores were as follows: 0, no lesion; 1, mild; 2, moderate; 3, severe. (*F–K*) VSV infection in NSUN2$^{+/-}$ and WT mice. The 4-6-wk-old SPF female WT mice and NSUN2$^{+/-}$ mice were intranasally inoculated with 10^6 plaque-forming units (PFU) of VSV. At day 3 postinoculation, all mice were euthanized, and VSV titers in lungs (*F*) and brain (*I*) were quantified by plaque assay. Total RNA was extracted from lung tissues for quantification of IFN-α and IFN-β mRNA by RT-qPCR (*K*). Representative lung histological images (*H*) and average score (*G*) from each group are shown. Average brain histology score from each group is shown (*J*). Scores were based on the severity of encephalitis. Scores were as follows: 0, no lesion; 1, mild; 2, moderate; 3, severe. Data were analyzed using a Student's *t* test (*$P < 0.05$, ***$P < 0.001$).

purpose, we knocked down NSUN2 in mice using vivo-phosphorodiamidate morpholino oligomers (vivo-MOs), which have been widely used for gene knockdown in animals (*SI Appendix*, Fig. S17*A*) (42). As expected, intranasal delivery of NSUN2-specific vivo-MO resulted in a significant reduction in NSUN2 mRNA in lungs relative to the control vivo-MO group ($P < 0.01$) (*SI Appendix*, Fig. S17*B*). RSV genome replication was significantly reduced in NSUN2-knockdown lungs from the NSUN2 vivo-MO–treated group ($P < 0.01$) (*SI Appendix*, Fig. S17*C*). Significantly less lung pathology was observed from the NSUN2 vivo-MO–treated group compared to the control vivo-MO group (*SI Appendix*, Fig. S17 *D* and *E*) ($P < 0.05$). Importantly, both IFN-α and IFN-β mRNA expression significantly increased in the NSUN2 vivo-MO–treated group compared to the control vivo-MO–treated group (*SI Appendix*, Fig. S17*F*) ($P < 0.01$ or 0.05).

Similar therapeutic effects were observed in VSV-infected mice. After intravenous delivery of vivo-MO to mice, NSUN2 mRNA was significantly reduced in lungs from the NSUN2 vivo-MO–treated group ($P < 0.05$) (*SI Appendix*, Fig. S17*G*). Importantly, VSV RNA replication was significantly reduced in lungs from the NSUN2 vivo-MO–treated group (*SI Appendix*, Fig. S17*H*) ($P < 0.01$), which was accompanied by a significant increase in both IFN-α and IFN-β mRNA (*SI Appendix*, Fig. S17*I*) ($P < 0.001$). The NSUN2 vivo-MO–treated group had significantly less lung pneumonia (*SI Appendix*, Fig. S17 *J* and *K*). We found approximately a 2 log reduction in VSV titer in brains from the NSUN2 vivo-MO–treated group (*SI Appendix*, Fig. S17*L*) ($P < 0.01$). The brain tissue from the control vivo-MO–treated group had mild to moderate encephalitis (*SI Appendix*, Fig. S17 *M* and *N*). In contrast, the brain tissue from the NSUN2 vivo-MO–treated group had no signs of encephalitis (*SI Appendix*, Fig. S17 *M* and *N*). These results illustrate that inhibition of NSUN2 in vivo reduces viral replication and pathogenesis.

Discussion

Our studies reveal a novel role of m^5C methylation in modulating host innate immunity that controls virus infection indirectly. A model consistent with our findings is depicted in Fig. 11. NSUN2 depletion increases and alters the m^5C methylome of host-derived RNAs, particularly ncRNAs including RPPH1, the RNA component RNase P complex. The increased level of RPPH1 and defects in m^5C methylation in RPPH1 probably enhance RNase P activity, which increases Pol III transcription, generating an increased level of regulatory small RNAs and lncRNAs, particularly the SRP RNAs including 7SL RNA. Under normal conditions, these regulatory lncRNAs are abundant and shielded by their protein-binding partners and thereby are not "visible" to RIG-I. Once NSUN2 is depleted, the increase in these abundant lncRNAs alters their molecular ratio versus their protein-binding partners, and then leads to an increase in unshielded lncRNAs in the cytoplasm, where they serve as ligands for RIG-I binding and signaling through the downstream adapter protein MAVS, activating the phosphorylation of IRF3, resulting in increased type I IFN. Although the IFN level in NSUN2-depleted cells is relatively low without any stimulant, the innate immune system has been in an "activated stage" with enhanced levels of pattern recognition receptors (PRRs; such as RIG-I and MDA5). Upon virus infection or stimulation with invaders, the increased PRRs quickly recognize these non-self RNAs [e.g., viral RNA and poly(I:C)], further amplifying IFN signaling and leading to a dramatically enhanced type I IFN which in turn inhibits virus propagation.

Using modified bisulfite sequencing and stringent cutoffs, we identified NSUN2-target m^5C methylation in tRNAs and several ncRNAs including RPPH1, scaRNA2, snoRNA 62A/62B, and vtRNA1-1 in both VSV- and RSV-infected A549 cells; most of these m^5C sites were also identified in previous studies using miCLIP in HEK293 cells (11), Aza-IP, and RNA bisulfite sequencing in HeLa cells (10, 12, 13). The miCLIP-based m^5C

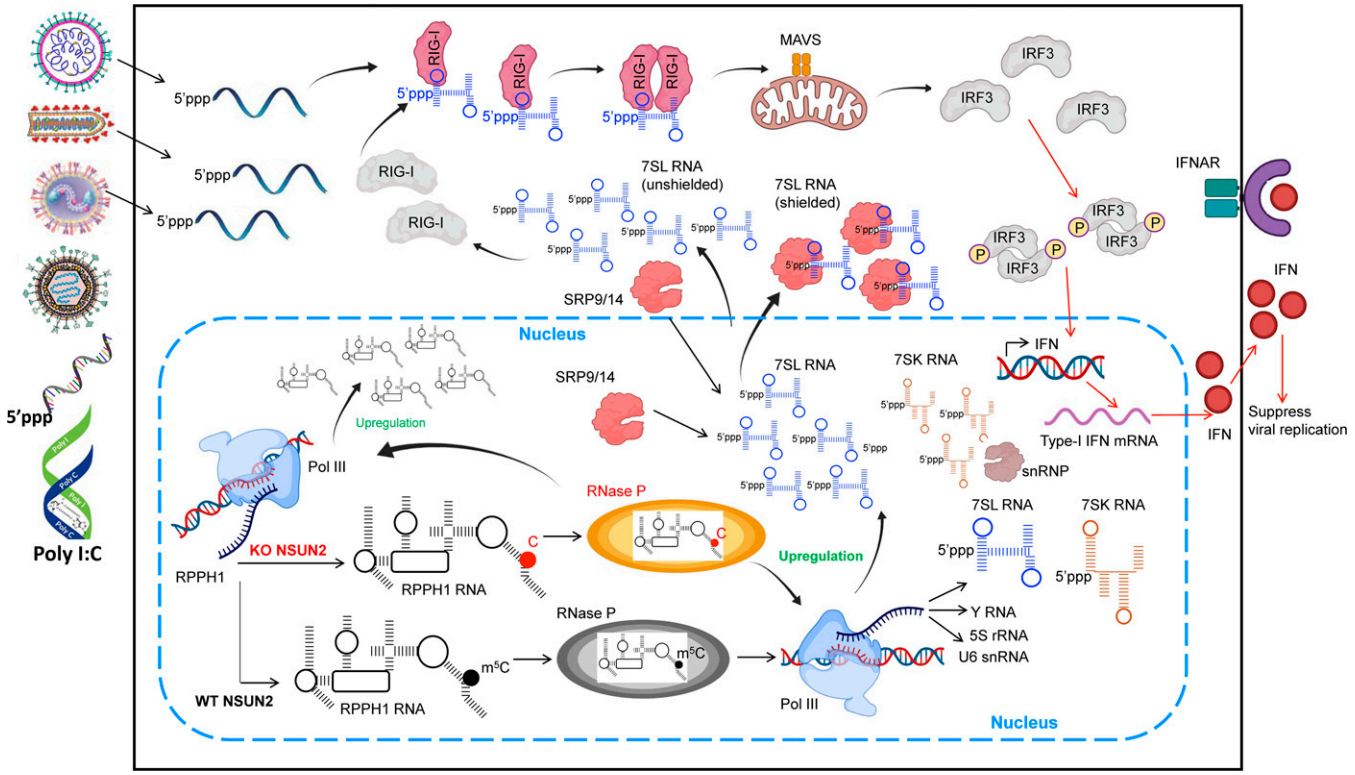

Fig. 11. Model of NSUN2 regulation of type I IFN signaling. Upon depletion of NSUN2 in A549 cells, the increase in RPPH1 expression and the decrease in m^5C modification in RPPH1 may lead to enhance Pol III activity via regulating RNase P enzymatic activity. The elevation of Pol III–transcribed RNAs, especially 7SL RNAs, leads to an increase in unshielded 7SL RNAs in the cytoplasm, which can be recognized by RIG-I, causing type I IFN signaling. Upon virus infection, the increased PRRs quickly recognize the invading non-self RNAs, further amplifying IFN signaling and leading to a dramatically enhanced type I IFN which in turn inhibits virus propagation.

sequencing in HEK293 cells also identified NSUN2 target sites in 7SK and two vtRNAs, vtRNA1.2, and vtRNA1.3 (11). For comparison, we also performed m^5C sequencing for RNA extracted from HIV-1–infected WT and NSUN2-KO THP-1 cells using our bisulfite-based method. Importantly, we identified the consistent m^5C site in RPPH1 RNA, which displayed ~60 and ~20% mutation ratios in WT and NSUN2-KO THP-1 cells, respectively (*SI Appendix*, Fig. S18). Compared to the A549 cells, the RPPH1 m^5C site in THP-1 cells shows a higher methylation. In THP-1 cells, we also confirmed the NSUN2-methylated m^5C site in vtRNA and hundreds of NSUN2-methylated m^5C sites on cytoplasmic tRNA (*SI Appendix*, Fig. S18). We identified 35 detectable m^5C sites on HIV viral RNA purified from THP-1 cells (*SI Appendix*, Table S1). Forty-six and 80% of the 35 sites overlap with the m^5C peaks on HIV-1 RNA from virus-infected human T lymphoblast cells (CEM cells) and virion RNA grown in CEM cells, respectively (24). These m^5C sequencing techniques consistently revealed the alternation of m^5C methylomes in ncRNAs regulated by NSUN2 in various cell types with or without virus infection.

Recent studies have suggested that depletion of NSUN2 suppresses replication of retroviruses [HIV-1 and murine leukemia virus (MLV)] (24, 25, 28). However, this anti-retroviral effect was proposed to be mediated through dysregulated m^5C methylation of the HIV-1 genomic RNA (24) such as inhibition of HIV-1 mRNA translation, ribosomal recruitment, and HIV-1 RNA alternative splicing (24). However, the potential role of IFN in the anti-retroviral activity was not determined in those studies. In sharp contrast, we found that the antiviral effects after NSUN2 depletion is driven by the enhanced IFN response via regulating the host RNA m^5C methylome and ncRNA expression, not by dysregulation of m^5C methylation of the viral RNA. Furthermore, this enhanced type I IFN response in NSUN2-depleted cells is independent of viral replication, as cells stimulated with viral genomic RNA or ploy(I:C) had a similar effect, suggesting that the higher activation of type I IFN is a general mechanism in response to other immunostimulants. Our study showed that NSUN2 is not responsible for adding m^5C to the RSV genome. Future study will determine whether other m^5C writer proteins (such as NSUN1, NSUN3–7, and DNMT2) can methylate RSV genome (*SI Appendix*, Table S2).

Notably, we found that Pol III transcription product lncRNAs such as 7SL RNAs are recognized by RIG-I. The lncRNAs are typically 200 to 350 nt in length, bear 5′-triphosphate, and form short Y-shaped dsRNA structure (43, 44), which are potential ligands for RIG-I. Under normal physiological conditions, these lncRNAs are masked and shielded by their protein partners, which prevent them from being detected by the innate immune surveillance apparatus. We observed a significant reduction in 7SL RNAs once NSUN2-depleted A549 cells were treated with MNase, suggesting that the unshielded lncRNAs are significantly increased, which are subsequently detected by RIG-I. Our findings are consistent with recent observations that many host-derived endogenous RNAs such as 5S ribosomal RNA pseudogene 141 (RNA5SP141), small RNA cleavage products of RNase L, exosomal 7SL1 RNA, and other lncRNAs have been shown to be recognized by PRRs, triggering an innate immune response (34, 45).

It remains unknown how NSUN2 depletion leads to an increased level of these regulatory ncRNAs, but presumably it is due to the increase in Pol III transcription activity. NSUN2 may indirectly regulate Pol III activity via controlling the m^5C methylation of RPPH1, the RNA subunit of RNase P, which is known to be required for transcription of various small RNA and ncRNA genes by Pol III (5, 35, 36, 40).

In summary, our study highlights a major gap in our understanding of the role of m^5C methylation in innate immunity in vitro and in vivo. Specifically, depletion of the m^5C writer protein decreases the host RNA m^5C in the methylome and enhances Pol III–transcribed lncRNAs that are recognized by RIG-I to trigger an enhanced innate antiviral immune response. Our study suggests that NSUN2 and m^5C machinery may be a new, broad-spectrum antiviral strategy.

Materials and Methods

All animals were housed within University Laboratory Animal Resources facilities of The Ohio State University under approved Institutional Animal Care and Use Committee guidelines (protocol no. 2009A0160-R3). Detailed descriptions of cell cultures, virus strains, reagents, antibodies, plasmids, mutagenesis, siRNAs and plasmid transfection, NSUN2-KO cell lines and HBE cultures, in vitro RNA transcription, viral infection, replication, gene expression, viral titration, real-time RT-PCR, Western blot, fluorescence microscopy and flow cytometry, IFN assay, immunoprecipitation assay, RNA isolation, bisulfite sequencing for m^5C site detection, RNA-seq, cellular dsRNA isolation and dsRNA-seq, identification of bisulfite-induced misincorporation, differential expression analysis, noncoding RNA transcription and stability assay, animal studies in WT and NSUN2 dificient mice, knockdown of NSUN2 in mice by vivo-MO, histology, and statistical analysis are provided in *SI Appendix*.

Data, Materials, and Software Availability. m^5C sequencing data have been deposited in the Gene Expression Omnibus (GEO) database (GSE174374) (46). All other study data are included in the article and/or *SI Appendix*.

ACKNOWLEDGMENTS. This work was supported by National Institutes of Health Grants R01AI090060 (to J.L.), P01 AI112524 (to M.E.P. and J.L.), R01 HG008688 and RM1 HG008935 (to C.H.), and R00 AI125136 (to A.S.). C.H. is an investigator of the Howard Hughes Medical Institute. We thank Michaela Frye (German Cancer Research Center) for $NSUN2^{+/-}$ mice and Jacob Yount (OSU) for the RIG-I plasmid.

Author affiliations: [a]Department of Veterinary Biosciences, College of Veterinary Medicine, The Ohio State University, Columbus, OH 43210; [b]Department of Chemistry, The University of Chicago, Chicago, IL 60637; [c]Department of Biochemistry and Molecular Biology, The University of Chicago, Chicago, IL 60637; [d]The Institute for Biophysical Dynamics, The University of Chicago, Chicago, IL 60637; [e]Center for Vaccines and Immunity, Abigail Wexner Research Institute, Nationwide Children's Hospital, Columbus, OH 43205; [f]Department of Microbiology, Molecular Genetics and Immunology, University of Kansas Medical Center, Kansas City, KS 66160; [g]Department of Pediatrics, College of Medicine, The Ohio State University, Columbus, OH 43205; [h]Department of Microbial Infection and Immunity, College of Medicine, The Ohio State University, Columbus, OH 43210; and [i]Howard Hughes Medical Institute, The University of Chicago, Chicago, IL 60637

Author contributions: Y.Z., L.-S.Z., V.M., R.K.S., X.L., A.S., C.H., and J.L. designed research; Y.Z., L.-S.Z., Q.D., P.C., M.L., E.L.K., V.M., J.X., R.K.S., X.L., Z.Z., E.C.-B., J.Q., M.E.P., A.S., C.H., and J.L. performed research; Y.Z., L.-S.Z., Q.D., E.C.-B., J.Q., M.E.P., C.H., and J.L. contributed new reagents/analytic tools; Y.Z., L.-S.Z., Q.D., P.C., M.L., E.L.K., Z.Z., A.S., C.H., and J.L. analyzed data; and Y.Z., L.-S.Z., C.H., and J.L. wrote the paper.

1. Q. Li *et al.*, NSUN2-mediated m5C methylation and METTL3/METTL14-mediated m6A methylation cooperatively enhance p21 translation. *J. Cell. Biochem.* **118**, 2587–2598 (2017).
2. B. S. Zhao, I. A. Roundtree, C. He, Post-transcriptional gene regulation by mRNA modifications. *Nat. Rev. Mol. Cell Biol.* **18**, 31–42 (2017).
3. Y. Fu, D. Dominissini, G. Rechavi, C. He, Gene expression regulation mediated through reversible m^6A RNA methylation. *Nat. Rev. Genet.* **15**, 293–306 (2014).
4. M. Lu *et al.*, N^6-methyladenosine modification enables viral RNA to escape recognition by RNA sensor RIG-I. *Nat. Microbiol.* **5**, 584–598 (2020).
5. M. Baer, T. W. Nilsen, C. Costigan, S. Altman, Structure and transcription of a human gene for H1 RNA, the RNA component of human RNase P. *Nucleic Acids Res.* **18**, 97–103 (1990).
6. V. Khoddami *et al.*, Transcriptome-wide profiling of multiple RNA modifications simultaneously at single-base resolution. *Proc. Natl. Acad. Sci. U.S.A.* **116**, 6784–6789 (2019).
7. T. Amort, A. Lusser, Detection of 5-methylcytosine in specific poly(A) RNAs by bisulfite sequencing. *Methods Mol. Biol.* **1562**, 107–121 (2017).
8. J. Liu, G. Jia, Methylation modifications in eukaryotic messenger RNA. *J. Genet. Genomics* **41**, 21–33 (2014).
9. M. Frye, B. T. Harada, M. Behm, C. He, RNA modifications modulate gene expression during development. *Science* **361**, 1346–1349 (2018).
10. X. Yang *et al.*, 5-methylcytosine promotes mRNA export–NSUN2 as the methyltransferase and ALYREF as an m^5C reader. *Cell Res.* **27**, 606–625 (2017).
11. S. Hussain *et al.*, NSun2-mediated cytosine-5 methylation of vault noncoding RNA determines its processing into regulatory small RNAs. *Cell Rep.* **4**, 255–261 (2013).
12. V. Khoddami, B. R. Cairns, Identification of direct targets and modified bases of RNA cytosine methyltransferases. *Nat. Biotechnol.* **31**, 458–464 (2013).
13. J. E. Squires *et al.*, Widespread occurrence of 5-methylcytosine in human coding and non-coding RNA. *Nucleic Acids Res.* **40**, 5023–5033 (2012).
14. K. E. Bohnsack, C. Höbartner, M. T. Bohnsack, Eukaryotic 5-methylcytosine (m^5C) RNA methyltransferases: Mechanisms, cellular functions, and links to disease. *Genes (Basel)* **10**, 102 (2019).
15. L. Trixl, A. Lusser, The dynamic RNA modification 5-methylcytosine and its emerging role as an epitranscriptomic mark. *Wiley Interdiscip. Rev. RNA* **10**, e1510 (2019).
16. F. Tuorto *et al.*, RNA cytosine methylation by Dnmt2 and NSun2 promotes tRNA stability and protein synthesis. *Nat. Struct. Mol. Biol.* **19**, 900–905 (2012).
17. L. Van Haute *et al.*, NSUN2 introduces 5-methylcytosines in mammalian mitochondrial tRNAs. *Nucleic Acids Res.* **47**, 8720–8733 (2019).
18. X. Chen *et al.*, 5-methylcytosine promotes pathogenesis of bladder cancer through stabilizing mRNAs. *Nat. Cell Biol.* **21**, 978–990 (2019).
19. F. Zou *et al.*, *Drosophila* YBX1 homolog YPS promotes ovarian germ line stem cell development by preferentially recognizing 5-methylcytosine RNAs. *Proc. Natl. Acad. Sci. U.S.A.* **117**, 3603–3609 (2020).
20. M. Frye, F. M. Watt, The RNA methyltransferase Misu (NSun2) mediates Myc-induced proliferation and is upregulated in tumors. *Curr. Biol.* **16**, 971–981 (2006).
21. J. Blaze *et al.*, Neuronal Nsun2 deficiency produces tRNA epitranscriptomic alterations and proteomic shifts impacting synaptic signaling and behavior. *Nat. Commun.* **12**, 4913 (2021).
22. D. T. Dubin, V. Stollar, Methylation of Sindbis virus "26S" messenger RNA. *Biochem. Biophys. Res. Commun.* **66**, 1373–1379 (1975).
23. S. Sommer *et al.*, The methylation of adenovirus-specific nuclear and cytoplasmic RNA. *Nucleic Acids Res.* **3**, 749–765 (1976).
24. D. G. Courtney *et al.*, Epitranscriptomic addition of m^5C to HIV-1 transcripts regulates viral gene expression. *Cell Host Microbe* **26**, 217–227.e6 (2019).
25. D. G. Courtney *et al.*, Extensive epitranscriptomic methylation of A and C residues on murine leukemia virus transcripts enhances viral gene expression. *MBio* **10**, e01209-19 (2019).
26. R. R. Dev *et al.*, Cytosine methylation by DNMT2 facilitates stability and survival of HIV-1 RNA in the host cell during infection. *Biochem. J.* **474**, 2009–2026 (2017).
27. B. A. Henry, J. P. Kanarek, A. Kotter, M. Helm, N. Lee, 5-methylcytosine modification of an Epstein-Barr virus noncoding RNA decreases its stability. *RNA* **26**, 1038–1048 (2020).
28. M. Eckwahl *et al.*, 5-methylcytosine RNA modifications promote retrovirus replication in an ALYREF reader protein-dependent manner. *J. Virol.* **94**, e00544-20 (2020).
29. M. Y. King, K. L. Redman, RNA methyltransferases utilize two cysteine residues in the formation of 5-methylcytosine. *Biochemistry* **41**, 11218–11225 (2002).
30. S. Shinoda *et al.*, Mammalian NSUN2 introduces 5-methylcytidines into mitochondrial tRNAs. *Nucleic Acids Res.* **47**, 8734–8745 (2019).
31. T. Huang, W. Y. Chen, J. H. Liu, N. N. Gu, R. Zhang, Genome-wide identification of mRNA 5-methylcytosine in mammals. *Nat. Struct. Mol. Biol.* **26**, 380–388 (2019).
32. H. Kleinert, A. Gladen, M. Geisler, B. J. Benecke, Differential regulation of transcription of human 7 S K and 7 S L RNA genes. *J. Biol. Chem.* **263**, 11511–11515 (1988).
33. R. Reichel, B. J. Benecke, Reinitiation of synthesis of small cytoplasmic RNA species K and L in isolated HeLa cell nuclei in vitro. *Nucleic Acids Res.* **8**, 225–234 (1980).
34. B. Y. Nabet *et al.*, Exosome RNA unshielding couples stromal activation to pattern recognition receptor signaling in cancer. *Cell* **170**, 352–366.e13 (2017).
35. R. Reiner, Y. Ben-Asouli, I. Krilovetzky, N. Jarrous, A role for the catalytic ribonucleoprotein RNase P in RNA polymerase III transcription. *Genes Dev.* **20**, 1621–1635 (2006).
36. C. Guerrier-Takada, K. Gardiner, T. Marsh, N. Pace, S. Altman, The RNA moiety of ribonuclease P is the catalytic subunit of the enzyme. *Cell* **35**, 849–857 (1983).
37. Y. H. Chiu, J. B. Macmillan, Z. J. J. Chen, RNA polymerase III detects cytosolic DNA and induces type I interferons through the RIG-I pathway. *Cell* **138**, 576–591 (2009).
38. B. Y. Nabet *et al.*, Exosome RNA unshielding couples stromal activation to pattern recognition receptor signaling in cancer. *Cell* **170**, 352–366.e13 (2017).
39. M. Xue *et al.*, Stable attenuation of human respiratory syncytial virus for live vaccines by deletion and insertion of amino acids in the hinge region between the mRNA capping and methyltransferase domains of the large polymerase protein. *J. Virol.* **94**, e01831-20 (2020).
40. M. G. Xue *et al.*, Viral N^6-methyladenosine upregulates replication and pathogenesis of human respiratory syncytial virus. *Nat. Commun.* **10**, 4595 (2019).
41. S. Blanco *et al.*, The RNA-methyltransferase Misu (NSun2) poises epidermal stem cells to differentiate. *PLoS Genet.* **7**, e1002403 (2011).
42. R. Rajsbaum, Intranasal delivery of peptide-morpholinos to knockdown influenza host factors in mice. *Methods Mol. Biol.* **1565**, 191–199 (2017).
43. A. Kuglstatter, C. Oubridge, K. Nagai, Induced structural changes of 7SL RNA during the assembly of human signal recognition particle. *Nat. Struct. Biol.* **9**, 740–744 (2002).
44. V. Siegel, P. Walter, Binding sites of the 19-kDa and 68/72-kDa signal recognition particle (SRP) proteins on SRP RNA as determined in protein-RNA "footprinting". *Proc. Natl. Acad. Sci. U.S.A.* **85**, 1801–1805 (1988).
45. J. J. Chiang *et al.*, Viral unmasking of cellular 5S rRNA pseudogene transcripts induces RIG-I-mediated immunity. *Nat. Immunol.* **19**, 53–62 (2018).
46. Y. Zhang, L.-S. Zhang, C. He, J. Li, Datasets for GSE174374. GEO. https://www.ncbi.nlm.nih.gov/geo/query/acc.cgi?acc=GSE174374. Deposited 26 September 2022.